PHYSICAL REVIEW C **88**, 034301 (2013)

Structure of unbound neutron-rich ^{9}He studied using single-neutron transfer

T. Al Kalanee,[1,2] J. Gibelin,[1,2,*] P. Roussel-Chomaz,[2] N. Keeley,[3] D. Beaumel,[4] Y. Blumenfeld,[4] B. Fernández-Domínguez,[2]
C. Force,[2] L. Gaudefroy,[2] A. Gillibert,[5] J. Guillot,[4] H. Iwasaki,[4] S. Krupko,[6] V. Lapoux,[5] W. Mittig,[2] X. Mougeot,[5] L. Nalpas,[5]
E. Pollacco,[5] K. Rusek,[3,7] T. Roger,[2] H. Savajols,[2] N. de Séréville,[4] S. Sidorchuk,[6] D. Suzuki,[4] I. Strojek,[3] and N. A. Orr[1]
[1]*LPC Caen, ENSICAEN, Université de Caen, CNRS/IN2P3, F-14050 CAEN Cedex, France*
[2]*GANIL, CEA/DSM-CNRS/IN2P3, BP55027, F-14076 Caen Cedex 5, France*
[3]*National Centre for Nuclear Research, ul. Andrzeja Sołtana 7, 05-400 Otwock, Poland*
[4]*IPN Orsay, IN2P3-CNRS, Université Paris Sud, F-91406 Orsay, France*
[5]*CEA-Saclay, DSM/IRFU SPhN, F-91191 Gif-sur-Yvette Cedex, France*
[6]*Flerov Laboratory of Nuclear Reactions, JINR, Dubna, RU-141980 Russia*
[7]*Heavy Ion Laboratory, University of Warsaw, ul. Pasteura 5A, PL-02-093 Warsaw, Poland*

(Received 29 April 2013; revised manuscript received 27 July 2013; published 3 September 2013)

The ^{8}He(d,p) reaction was studied in inverse kinematics at 15.4A MeV using the MUST2 Si-CsI array in order to shed light on the level structure of ^{9}He. The well known ^{16}O$(d,p)^{17}$O reaction, performed here in reverse kinematics, was used as a test to validate the experimental methods. The ^{9}He missing mass spectrum was deduced from the kinetic energies and emission angles of the recoiling protons. Several structures were observed above the neutron-emission threshold and the angular distributions were used to deduce the multipolarity of the transitions. This work confirms that the ground state of ^{9}He is located very close to the neutron threshold of ^{8}He and supports the occurrence of parity inversion in ^{9}He.

DOI: 10.1103/PhysRevC.88.034301 PACS number(s): 21.10.Jx, 21.10.Pc, 21.10.Tg, 25.45.Hi

I. INTRODUCTION

Neutron-rich $N = 7$ isotones are of particular interest because of their level sequence, which differs from that predicted by the shell model for nuclei near stability [1]. The standard shell model generally predicts a $J^\pi = 1/2^-$ ground state (g.s.) for $N = 7$ nuclei. This is true for ^{15}O and ^{13}C, but ^{11}Be presents parity inversion with a $1/2^+(\nu 2s_{1/2})$ ground state [2]. This parity inversion was predicted for the first time by Talmi and Unna in 1960 [1]: they showed that parity inversion for ^{11}Be can be predicted from linear extrapolation of the $p_{1/2}$-$s_{1/2}$ energy in ^{13}C (3.09 MeV) and the corresponding difference between the center of mass associated states in ^{12}B (1.44 MeV). Hence the $s_{1/2}$ state was predicted to be the g.s. of ^{11}Be at 0.21 MeV below the $p_{1/2}$ level. Recent results for ^{10}Li [3–6] also confirm the observation of a virtual s state close to the neutron emission threshold and the presence of a resonance around 0.5 MeV.

The first results for the unbound ^{9}He nucleus were obtained by Seth *et al.* in 1987 via the double-charge exchange reaction ^{9}Be$(\pi^-,\pi^+)^9$He [7]. The lowest energy state observed was considered to be the ground state at 1.13(10) MeV above the neutron threshold with a width of $\Gamma = 0.42(0.1)$ MeV and a $1p_{1/2}$ configuration. Two excited states were observed: the first excited state was identified as a $2s_{1/2}$ state at 2.33(0.1) MeV with $\Gamma = 0.42(0.1)$ and the second as a $5/2^+$ or $3/2^-$ state at 4.93(0.1) MeV [$\Gamma = 0.5(0.1)$ MeV]. There was also a possible state at 8.13 MeV with $\Gamma = 0.55(0.1)$ MeV.

The ^{9}Be$(^{13}$C$,^{13}$O$)$ reaction was studied by von Oertzen *et al.* [8] and Bohlen *et al.* [9]. Despite low statistics, a state at 1.13 MeV above the neutron threshold and another state at 4.93 MeV were observed. The same authors [8,10] also investigated the ^{9}Be$(^{14}$C$,^{14}$O$)^9$He reaction. A $J^\pi = 1/2^-$ state was proposed for the ground state at 1.27 MeV above the neutron threshold with $\Gamma = 0.1(6)$ MeV. Three excited states were found at 2.37(10) [with $\Gamma = 0.7(2)$ MeV], 4.3(10), and 5.25(10) MeV, respectively. Note that recently the heavy-ion double-charge exchange reaction ^{9}Be$(^{18}$O$,^{18}$Ne$)^9$He [11] was investigated but the results do not show any structure in ^{9}He.

In these three studies, the state identified as the ground state was assigned a $J^\pi = 1/2^-$ spin-parity, leading to the conclusion that there is no parity inversion in ^{9}He, thus breaking the systematics started with ^{11}Be and ^{10}Li. These results were consistent with theoretical studies at the time [12,13], however they are in contradiction with more recent calculations [14–18].

More recently Barker [19] showed that the small width of the $1/2^-$ level ($\Gamma = 0.42$ MeV [7] and $\Gamma = 0.1$ MeV [8]) is inconsistent with a single-particle state. According to Barker's calculations, the $1/2^-$ single-particle width for ^{8}He + n should be about 1 MeV.

The two-proton knock-out reaction from ^{11}Be at 28A MeV studied by Chen *et al.* [17] was the first experiment to identify a state at a lower energy than the earlier experiments. This "new" ground state at around 0.2 MeV above the ^{8}He + n threshold was assigned a $2s_{1/2}$ configuration, indicating for the first time parity inversion in the ^{9}He nucleus. The scattering length a_s found by Chen was $a_s \leqslant -10$ fm, corresponding to a virtual state of energy $E_r \lesssim 0.2$ MeV. These results were consistent with shell model calculations undertaken by Warburton and Brown [20].

Later, the C$(^{11}$Be$,^8$He$+n)X$ reaction at 35A MeV was studied by Al Falou *et al.* [5,21]. The neutron-^{8}He relative energy spectrum could be explained by a virtual s state of scattering length $-3 \lesssim a_s \lesssim 0$ fm, consistent with no or at

---

[*] gibelin@lpccaen.in2p3.fr

most a very weak final state interaction. Al Falou *et al.* also studied the C(^{14}B,^{8}He $+ n)X$ reaction at 35A MeV the results of which were consistent with a very weakly interacting s state and a resonance at $E_r \approx 1.3$ MeV with a width of $\Gamma \approx 1$ MeV.

The most recent results on ^{9}He using this type of reaction were published by Johansson *et al.* [22]. They used the ^{1}H(^{11}Li,^{8}He $+ n$) knock-out reaction at 280A MeV. Their work shows dominant s-wave scattering at low energy with $a_s = -3.17(66)$ fm in addition to two resonances at 1.33(8) MeV [$\Gamma = 0.1(6)$ MeV] and 2.42(10) MeV [$\Gamma = 0.7(20)$ MeV] above the neutron threshold. Given the reaction used and the very small scattering length, the low energy structure was attributed to a threshold effect rather that a true state.

A study of the isobaric analog states of ^{9}He in ^{9}Li was performed by Rogachev *et al.* [23] via the elastic scattering of ^{8}He on protons at around 7A MeV. The experimental setup did not allow the lowest energy states to be observed but three states were seen above threshold: a $1/2^-$ or $3/2^-$ state at 1.1 MeV with a width of $\Gamma < 0.1$ MeV, a second $3/2^-$ (or $1/2^-$) state at 2.2 MeV [$\Gamma = 1.1(0.4)$ MeV], and a $(5/2^+, 3/2^+)$ state at 4.0 MeV with $\Gamma = 0.24(0.1)$ MeV.

Finally, the structure of ^{9}He has been studied using transfer reactions. Fortier *et al.* [24] employed the $d(^8\mathrm{He},p)^9\mathrm{He}$ reaction at a beam energy of 15.3A MeV. The use of eight MUST [25] telescopes at backward angles enabled laboratory angles (θ_{lab}) from 110° to 170° to be covered. This study found three states at ≈0 MeV, 1.3 MeV, and 2.3 MeV and two other possible states at higher energies [26]. The angular distributions measured for the first two states suggest an inversion between the $1/2^+$ and $1/2^-$ levels, but the very limited statistics obtained (especially for the peak around the neutron threshold) made it difficult to draw definite conclusions.

The same reaction was studied by Golovkov *et al.* [27], using a ^{8}He beam at the higher energy of 25A MeV. The presence of a virtual state with a scattering length $a_s > -20$ fm was inferred from the large forward-backward asymmetry of the spectra. Two excited states were observed: a $1/2^-$ state at 2 MeV with $\Gamma \sim 2$ MeV and a $5/2^+$ state at $\geqslant 4.2$ MeV with $\Gamma > 0.5$ MeV. It is worth noting that the width of the first excited state in this work is much larger than in the majority of the previous experiments.

The present experiment used the same reaction and an almost identical energy to Fortier *et al.* [24]—$d(^8\mathrm{He},^9\mathrm{He})p$ at 15.4A MeV—and benefited from an increased of the ^{8}He beam intensity and an improved angular coverage possible with the new MUST2 array [28].

II. EXPERIMENT

The experiment was performed at the GANIL facility and was part of the first MUST2 campaign [29,30]. A secondary ^{8}He beam at 15.4A MeV was produced by the SPIRAL1 ISOL facility [31] via the fragmentation of a 75A MeV ^{13}C beam in a thick carbon target. After reacceleration and purification the beam was delivered to a deuterium-enriched polyethylene targets $(\mathrm{CD}_2)_n$ of 320 μg/cm^2 or 550 μg/cm^2 thickness. (Here, and in the following, 'D' denotes deuterium, '^{2}H'.) The horizontal and vertical size of both targets was 4 cm and 3 cm, respectively. The experimental setup is shown in Fig. 1. For more details see Refs. [32–35].

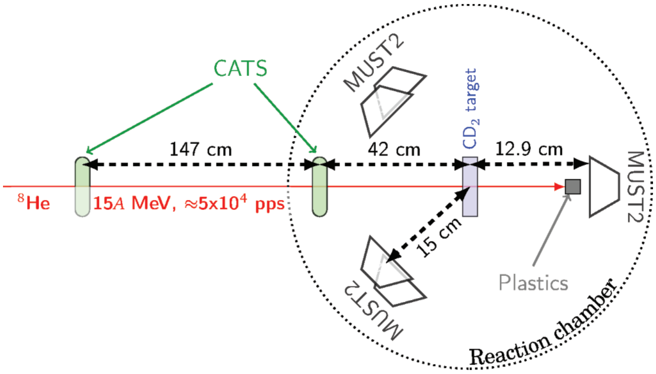

FIG. 1. (Color online) Schematic diagram of the experimental setup. Trapezium shapes represent MUST2 modules.

The beam spot on the target and the incident angles of incoming particles were monitored event-by-event using two sets of multiwire low pressure chambers, CATS [36]. The typical size of the ^{8}He beam was 3.3 mm (FWHM) and the range of incoming angles was 26 mrad (FWHM).

The energies and angles of the recoiling protons were measured by an array of four MUST2 telescopes [28] located upstream of the target. Each telescope, with an active area of 10×10 cm^2, consisted of a 300-μm thick double-sided Si strip detector (DSSSD) and a 4-cm thick 16-fold CsI calorimeter, which provided energy-loss (ΔE) and residual-energy (E) measurements, respectively. The DSSSDs were divided into 128 strips in both the x and y directions, thus providing position information. The emission angle of the recoiling particles was obtained by combining this information with the angle and position of the incoming ^{8}He on the target.

The acceptance of the array was estimated using a Monte Carlo simulation which took into account the detector geometry and the beam profile. For the proton at backward angle, the setup covered laboratory (center-of-mass) angles between 120°–170° ($\sim$$2.7^\circ$–$21.4^\circ$). The acceptance has a maximum value of $\sim 80\%$ at $\theta_{\mathrm{lab}} = 135^\circ$–$160^\circ$ ($\theta_{\mathrm{c.m.}} \sim 6^\circ$–$16^\circ$), while it gradually decreases toward smaller or larger angles. The total kinetic energy was obtained from the proton energy information, to which a correction was applied based on the calculated energy loss in the target. This correction depends on both energy and angle and was typically of the order of 50 keV.

The beam particles and forward emitted ^{8}He from the in-flight decay of ^{9}He were detected by a 20×20 mm^2, 1 mm thick, NE102 plastic scintillator located 11 cm downstream of the target and covering $\theta_{\mathrm{lab}} = 0^\circ$ to 5.6° (representing 97% of the reconstructed events). Larger angles up to 6.5° were covered by a fifth MUST2 telescope located 19 mm behind the plastic scintillator.

III. ANALYSIS

As noted above, the reaction position on the target was reconstructed from the position measurements made using the two CATS detectors on an event by event basis. Only events where both CATS had fired were selected for analysis in order to reconstruct the trajectory of the beam particle and to ensure that the beam hit the target.

The ranges of the protons of interest (emitted from the transfer reactions populating either ^{17}O or ^{9}He) being such that all were expected to stop in the first 300 μm stage of the telescope, we rejected all events where any CsI directly behind the measured impact position in a DSSSD had fired. Proton identification was performed using the energy-time of flight method [32].

The presence of the plastic scintillator located downstream of the target allowed us to perform coincidences with all beam-like particles and potentially outgoing ^{8}He (no isotope separation was however possible). The ^{8}He beam ions that stopped in the plastic scintillator emitted β particles through their decay ($T_{1/2} \sim 120$ ms) and produced reaction induced protons that could be seen in the backward telescopes. The β particles being of low energy and uncorrelated to the beam they could be easily identified and eliminated at the cost of losing very low energy protons below 600 keV, close to the detection threshold of MUST2. The second contamination (protons) was in coincidence with the beam but as plastic scintillator was located 11 cm after the CD$_2$ target, these particles came at least 5 ns after the protons of interest. The MUST2 time resolution of 500 ps was then sufficient to disentangle them, provided they did not punch through the first layer of the telescope.

Additional conditions were employed: we selected events with multiplicity one for all backward telescopes; we rejected events where the energies collected from the two sides of the DSSSD were not equal (within the resolution) and, finally, the proton energies were restricted to kinematically reasonable ones, within the experimental resolution.

The scattering angle was deduced from the proton hit position on MUST2, the reaction point on target and the angle of incidence of the beam. The excitation energy, E_4^*, was calculated using

$$E_4^* = \sqrt{(T_1 + m_1 + m_2 - T_3 - m_3)^2 - P_1^2 - P_3^2 + 2P_1P_3\cos(\theta)} - m_4, \tag{1}$$

where the indices $i = 1, 2, 3, 4$ stand, respectively, for the beam, deuteron, proton, and nucleus of interest (^{9}He or ^{17}O), and P_i are the momenta, T_i the kinetic energies, and m_i the rest masses. The masses were taken from Refs. [37] ($A = 16$ and 17) and [38] (^{8}He). The mass of the ^{9}He was defined as the sum of the rest masses of ^{8}He and a free neutron (see below).

In order to test both our understanding of the setup and our analysis procedures, a test measurement of the ^{16}O$(d,p)^{17}$O reaction at 15.5A MeV was made in inverse kinematics. Note that in this case, the MUST2 module and the plastic detector at 0° were removed and no recoil identification was possible. Figure 2 presents the missing mass spectrum of ^{17}O obtained with the 550 μg/cm^2 target. Two states around 0 and 0.9 MeV are clearly separated, and two other states around 5.5 MeV can clearly be distinguished. Although other structures are present at higher energies we focus on these four states for which results from transfer the same reactions are available in the literature [39,40]. To refine our analysis we took into account two physical backgrounds: a three-body phase space simulating the deuteron break-up and a background due to reactions of the ^{16}O beam with the carbon present in the CD$_2$ target.

Using Gaussian distributions for the states below the neutron threshold $S_n = 4.1$ MeV and "Voigt profiles" [41] for the states above, we obtained the energies listed in Table I. We compared these results with tabulated and previously published values, in particular the work of Darden *et al.* [40] and Cooper *et al.* [39] (focusing on the latter as having the closest comparable conditions to our experiment, i.e., 18A MeV incident energy deuteron beam). We conclude from the energies listed in this table that our setup, calibration and analysis procedure reproduce with an accuracy better or equal to 5 keV the energies of the ground state and the first three excited single-particle states of ^{17}O. In addition, taking into account the experimental resolution deduced from simulations, the $\Gamma = 70$ keV width of the 5084 keV unbound state is reproduced.

For each state, we determined the integral above the background for a range of c.m. angles. Taking into account the beam exposure and correcting for the acceptance and dead time, differential angular distributions were constructed. Standard finite-range distorted wave Born approximation

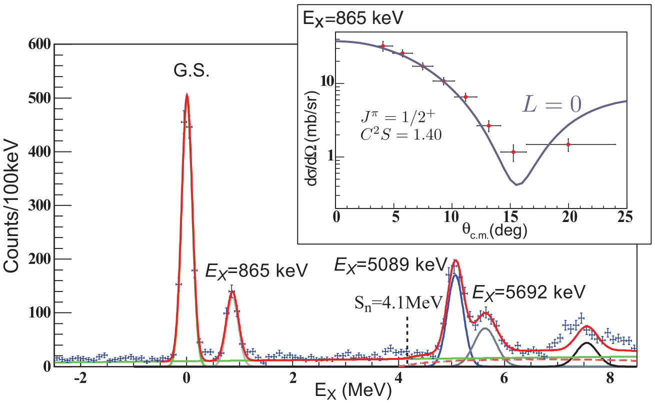

FIG. 2. (Color online) Experimental missing mass spectrum for the ^{16}O$(d,p)^{17}$O reaction in inverse kinematics. Dashed line (brown): three-body phase space. Thin solid line (green): background from reactions of the beam with the carbon of the CD$_2$ target. Inset: sample angular distribution for the first excited state, compared to a DWBA calculation.

TABLE I. Comparison between the results for ^{16}O$(d,p)^{17}$O in inverse kinematics and the adopted excitation energies (E_x) and previously published spectroscopic factors (C^2S) for the observed states. The uncertainties on the C^2S for this work here are estimated to be of the order of ±20% (see text).

J^π	E_x(keV)	C^2S	This work	
	(Adopted values [37])	(Refs. [39,40])	E_x	C^2S
$5/2^+$	0	1.07 – 0.84	5 ± 2	0.7
$1/2^+$	870.73 ± 0.10	1.14 – 0.91	865 ± 9	1.4
$3/2^+$	5084.8 ± 0.9	1.2	5089 ± 1	0.8
$7/2^-$	5697.26 ± 0.33	0.15	5692 ± 7	0.13

(DWBA) calculations were carried out using the code FRESCO [42]. These employed the same global deuteron and neutron optical model parameters for the distorting potentials in the entrance and exit channels, respectively, as used in the $d(^8\mathrm{He},p)$ calculations described later. The binding potentials for the $\langle d|n+p\rangle$ and $\langle ^{17}\mathrm{O}|^{16}\mathrm{O}+n\rangle$ overlaps also employed the same parameters as for the $d(^8\mathrm{He},p)$ calculations, the $^{16}\mathrm{O}+n$ values being similar to those of Refs. [39] and [40].

The four angular distributions obtained in the test measurement were well reproduced and the resulting angular distribution for the first excited state is shown, as an example, in the insert of Fig. 2. This demonstrates the validity of our experimental approach. Note that a systematic 10% error was assigned to the cross sections to take into account the effect of the uncertainties in: target thickness, detector efficiencies, and solid angles.

Finally, the corresponding spectroscopic factors C^2S were deduced by the normalization of the DWBA calculations to the measured angular distributions. The error on the normalization due to statical and systematic errors are ∼ 10%, and the uncertainties arising from the choice of potential in the DWBA calculations are estimated to be ∼ 20% [43]. Table I lists the C^2S, which are in reasonable agreement with those taken from the literature.

IV. RESULTS

The analysis procedure for the $d(^8\mathrm{He},{}^9\mathrm{He})p$ measurement were identical to the test experiment. The missing mass spectrum is presented in Fig. 3. Since the experimental resolutions obtained with the 320 and 550 μg/cm^2 targets were similar, we present here the sum of the spectra obtained with both targets. Note that here the rest mass m_4 in Eq. (1) is defined as the sum of the ^{8}He and free neutron rest masses. The calculated missing mass energy (denoted here as E_r) is thus defined from the neutron threshold of ^{9}He.

Two peaks can clearly be seen: one approximately 200 keV above threshold which we identified as g.s. and another around 1.5 MeV. We also observe a shoulder around 3 MeV. Given that the broad structure around 6 MeV is related to the proton energy cutoff and therefore not a real state, we concluded that the shoulder around 3 MeV is due to a second excited state. The presence and the position of the two excited states are compatible with several previous reports [7,8,23,24,26].

Using these energies as a first estimate of the resonance energies of the states, a fit was performed employing “Voigt profiles” [41]. The Lorentzian widths Γ are energy dependent $\Gamma = \Gamma_0\sqrt{\frac{E}{E_R}}$ [44]. The Gaussian component takes into account the experimental energy resolution. The widths were deduced from the results for the $^{16}\mathrm{O}(d,p)$ test measurement at the corresponding proton energy. Only the last structure around 6 MeV was considered as a simple Gaussian function. Physical backgrounds associated with three-, five-, and seven-body phase spaces corresponding to $^8\mathrm{He}+d \rightarrow {}^8\mathrm{He}+p+n$, $^6\mathrm{He}+p+3n$, and $^4\mathrm{He}+p+5n$ were taken into account. Finally, a linear background arising from reactions of the beam with the carbon of the target and reactions in the plastic scintillator beam stopper was added. The results are listed in Table II.

We will discuss these results in detail in the next section, although we note here that the ground state of ^{9}He is found at 180 ± 85 keV above the neutron threshold. This is compatible with the other (d,p) reaction [26,27] studies. Both the position and the rather small width of the first excited state are also compatible with several previous experiments [8,10,22,23,26].

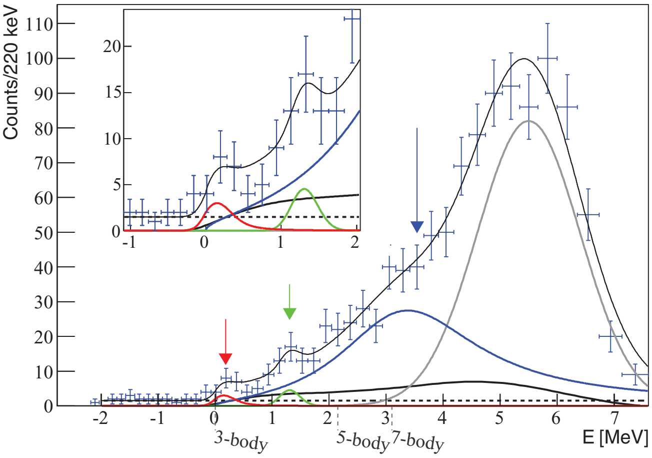

FIG. 3. (Color online) Experimental missing mass spectrum for the $(p,{}^8\mathrm{He})p$ reaction which is described with three states: ground state (red), first excited (green), and second excited (blue) states. The solid gray line models the acceptance cutoff. The solid black line denotes the sum of the three-, five-, and seven-body phase space contributions, whose respective breakup energies are noted. The dotted line indicates the physical background due to reactions of the beam with the plastic scintillator. The thin solid line is the sum of all contributions. The region around the threshold is shown in the inset.

TABLE II. Position and width of ^{9}He states obtained in this work. Spectroscopic factors were deduced using DWBA calculations (see text), the uncertainties originate from the different Woods-Saxon n + ^{8}He binding potentials used in the calculations.

E_r(keV)	Γ(keV)	C^2S			
		$p_{1/2}$	$p_{3/2}$	$d_{3/2}$	$d_{5/2}$
180 ± 85	180 ± 160				
1235 ± 115	130^{+170}_{-130}	0.02−0.05	0.01−0.03	0.006−0.01	0.005−0.007
3420 ± 780	2900 ± 390			0.03−0.04	0.02−0.03

The second excited state is slightly higher in energy than the average of previous experimental observations [7,8,22,23,26,27]. This could be due to the uncertainty in the shape of the structure located at 6 MeV, and a deviation of up to several hundred keV might be possible. The error on its position has been estimated by assuming different widths for the 6 MeV structure.

The experimental angular distributions for these three states are presented in Fig. 4. Error bars take into account uncertainties due to the subtraction of the different backgrounds. These angular distributions are compared with the results of full finite range DWBA calculations, similar to those carried out for the $d(^{16}\mathrm{O},p)^{17}\mathrm{O}$ reaction. The normalization for each energy and transferred angular momentum L was obtained with a log-likelihood fit.

The entrance channel $d+$ ^{8}He optical model potential was calculated using the global parameters of Daehnick *et al.* [45] and the exit channel $p+$ ^{9}He potentials employed the systematics of Koning and Delaroche [46]. The deuteron internal wave function, including the small D-state component, was calculated using the Reid soft-core interaction [47] as the neutron-proton binding potential. We used the weak binding energy approximation (WBEA) where the ^{9}He internal wave functions were calculated by binding the neutron to the ^{8}He core with a standard Woods-Saxon potential with reduced radius $r_0 = 1.25$ fm, and diffusivity $a_0 = 0.65$ fm, the well depths being adjusted to give a binding energy of 0.0001 MeV in all cases. Note that test calculations were performed with different sets of (r_0, a_0) values with ranges of 1.25−1.50 and 0.65−0.75, respectively, without noticeable effect on our conclusions.

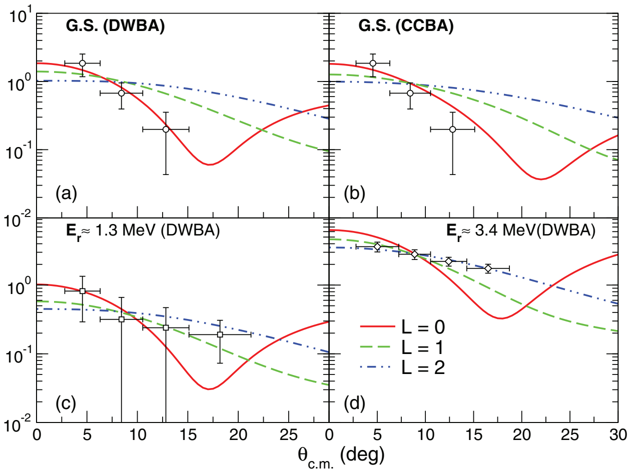

FIG. 4. (Color online) Angular distributions for the ground state (a) and the two first excited states of ^{9}He [(c) and (d)] compared to $L = 0, 1, 2$ (respectively red, green, and blue) DWBA calculations. (b) Angular distribution of the g.s. compared to CCBA calculations.

We chose to employ the WBEA to calculate the $n+$ ^{8}He overlaps for two reasons: firstly, when the unbound neutron is in a relative s state with respect to the ^{8}He core this results in a virtual state rather than a conventional resonance, due to the absence of either a Coulomb or a centrifugal barrier in the "binding" potential, thus rendering a more sophisticated modeling of the form factor for such states problematic. Secondly, while states with $L > 0$ may be modeled in FRESCO as true resonances with finite widths, in practice it is often difficult to achieve consistent results using this procedure. We therefore chose to use the WBEA to calculate all the $n+$ ^{8}He overlaps for the sake of consistency.

The procedure adopted was to perform calculations assuming angular momentum $L = 0$, 1, and 2 for the neutron relative to the ^{8}He core for all three states, and to compare the resulting angular distributions to the experimental points to deduce the best-fit values of L, thus providing clues as to the spin-parities of the respective states in ^{9}He, as well as spectroscopic factors. All calculations included the full complex remnant term and thus yielded identical results for either post- or prior-form DWBA.

Since the incident ^{8}He energy is relatively high, the influence of deuteron breakup effects could be important. To test this we performed a coupled-channels Born approximation (CCBA) calculation for stripping to the ground state of ^{9}He. The CCBA calculation was similar in all respects to the DWBA calculations with the exception that the entrance channel optical potential was replaced by a continuum discretized coupled channels (CDCC) calculation similar to that described in Ref. [48]. The necessary diagonal and transition potentials were calculated using Watanabe-type folding based on the global nucleon optical potential of Ref. [46] and the deuteron internal wave function of Ref. [47]. As Fig. 4(b) shows, the shapes of the $L = 0, 1, 2$ angular distributions are almost identical to those for the corresponding DWBA calculations, suggesting that the influence of deuteron breakup on the shape of the angular distribution is small in this case, justifying our use of the DWBA to infer spins and parities.

V. DISCUSSION

We present the ^{9}He states obtained in the present work together with all published results in Fig. 5. This confirms

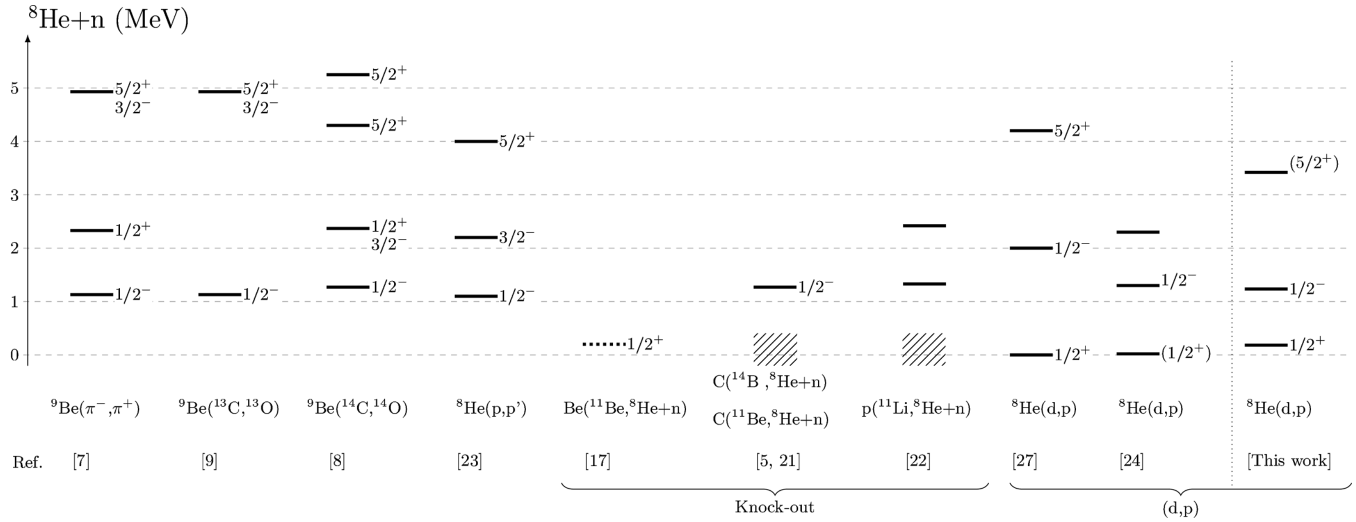

FIG. 5. Summary of all experimental results for ^{9}He, up to 5 MeV excitation energy. Solid lines represent states with well defined resonance. Dashed lines or hashed areas represent low-lying structures described by virtual s-wave states (see text for details).

the presence of a state in ^{9}He very close ($\sim$200 keV) to the neutron emission threshold—previously observed in (d, p) reactions [24,27]—that we have identified as the ground state. Different theoretical angular distributions for this state assuming different transferred angular momenta ($L = 0$, 1, or 2) calculated in both the DWBA and the CCBA formalisms are compared with experiment in Figs. 4(a) and 4(b). The experimental data present a sharp drop with increasing angle, characteristic of an $L = 0$ transition. Consequently, despite the very limited statistics, the present data support the contention that the lowest lying state in ^{9}He is $1/2^+$.

The present work is also compared in Fig. 5 with experiments utilizing knock-out reactions to study ^{9}He. For states close to the neutron threshold results were obtained in terms of scattering lengths: $a_s = -10$ fm [17], $a_s \geqslant -3$ fm [5], and $a_s = -3.17(66)$ fm [22]. Assuming that the low-lying structure observed is a resonance, a corresponding energy E_r is calculated and shown in Fig. 5. However, in this section we prefer to compare scattering lengths and since the g.s. is close to the neutron threshold we use the relation $E_r \approx \frac{\hbar^2}{2\mu a_s^2}$ [17] (where μ is the reduced mass for the neutron + ^{8}He system) to obtain the corresponding value $a_s \approx -12 \pm 3$ fm for the scattering length from this work. This scattering length is comparable to the result of Chen *et al.* [17] but is not compatible with the weakly interacting s-wave strength found both by Al Falou *et al.* [5] and Johansson *et al.* [22]. This may suggest, as noted by Johansson *et al.* [22], that the accumulation of strength close to the neutron threshold observed in these two experiments is inherent to the reaction and experimental conditions and not the observation of a well defined s-wave g.s.

The weak binding energy approximation used to calculate the theoretical angular distributions involves the use of a low binding energy (here 0.0001 MeV) to enable the calculation of the form factor in the usual way for unbound states while retaining the correct excitation energy for the "kinematical" part of the calculation. For $L = 0$ states strong variations in the calculated absolute cross section are observed as a function of the choice of the binding energy and it is therefore impossible to extract meaningful spectroscopic factors from the DWBA calculation in such cases. However, it is possible to estimate a value from the single-particle width. Using the prescriptions of Lane and Thomas [44] we find $\Gamma_{sp} \approx 2700$ keV for $E_r = 180$ keV. Experimentally $\Gamma = 180 \pm 160$ keV, which corresponds to a spectroscopic factor smaller than $\sim$0.13. Our calculation may however be too crude and more appropriate theoretical approaches are necessary to confirm this estimation.

It is more difficult to deduce the nature of the first excited state observed here at around 1.3 MeV above threshold from its angular distribution. Within the experimental uncertainties both the $L = 1$ and $L = 2$ calculations reproduce the data [Fig. 4(c)]. Our angular distribution is compatible with the $J^\pi = 1/2^-$ spin-parity assigned in most of the previous studies (Fig. 5). The small width measured here ($\Gamma = 130 \pm 170$ keV) corroborates several previous results [8,10,21–23]. The values of the corresponding spectroscopic factors (Table II) vary by a factor of up to 3 depending on the DWBA input parameters, but it is worth noting that all of them are substantially smaller than 1 (of the order of 0.05 for $L = 1$). This indicates that the first excited state is of a strongly mixed nature in agreement with the small observed width. From the analysis of this width, Barker [19] found spectroscopic factors $C^2S < 0.1$. Here, a calculation using the Lane and Thomas prescription [44] gives a single-particle width of 2.4 MeV for an $L = 1$ resonance at 1.25 MeV. From the observed width a spectroscopic factor of $C^2S \approx 0.06$ is deduced, in agreement with that extracted from the experimental angular distribution.

The excited state found here at around 3.5 MeV shows a smoothly decreasing angular distribution of $L = 2$ character [Fig. 4(d)]. Due to the large uncertainties in its energy ($\approx$800 keV), this state could be compared to the $5/2^+$ state found at around 4 MeV in Refs. [23,27]. The small corresponding spectroscopic factors suggest that this state is also strongly mixed. However, we extracted a width of the order of 3 MeV. Such a large width for decay to the ground state of ^{8}He would indicate a large spectroscopic factor but the measured cross section is compatible with an upper limit of $C^2S \lesssim 0.05$. We note that the cross section would be even smaller for a particular state if several states are present. To render these observations compatible, considering that this state is located above the $4n$ threshold, a strong decay branch to the ^{8}He 2^+ state is necessary.

Finally, only a few theoretical calculations are available for ^{9}He and we concentrate here on recent results. It is interesting to note that none of the recent calculations of the no core shell model [49] or the unified shell model approach [50] predict parity inversion, both suggesting a $1/2^-$ ground state. Only Otsuka *et al.* [18], within a more standard shell-model framework, are able to account for the inversion with the help of a strong attractive monopole interaction.

VI. CONCLUSIONS

We have investigated the ^{8}He(d,p) neutron stripping reaction in inverse kinematics at $15.4A$ MeV to explore the structure of the unbound neutron-rich nucleus ^{9}He. Despite limited statistics the angular distribution for the state observed very close to the $^8\text{He} + n$ threshold (180 ± 85 keV above) supports the contention that the ground state spin-parity of ^{9}He is $1/2^+$, thus confirming the parity inversion. Two excited states were observed: the first lies approximately 1.3 MeV above the neutron threshold and is compatible with $J^\pi = 1/2^-$, exhibiting at the same time a strong mixed nature. A second state at ∼3.5 MeV above threshold presents an $L = 2$ angular distribution, suggesting a $3/2^+$ or $5/2^+$ spin-parity assignment.

The present analysis suggests that in the excitation energy range up to 5 MeV in ^{9}He there is no state with a strong component of a single neutron coupled to a core of ^{8}He in its ground state. This is a qualitative change from ^{7}He, where the ground state has a large spectroscopic factor for $^6\text{He}_{\text{g.s.}}$ coupled to a single neutron. The large width of the 3.5 MeV state for decay to the 2^+ state in ^{8}He is compatible with the assumption that this state has a strong component of an excited $^8\text{He}(2^+)$ core coupled to a single neutron.

ACKNOWLEDGMENTS

We wish to thank the GANIL technical staff. N.K. and K.R. gratefully acknowledge receipt of a COPIGAL grant. We would also like to thank F. Gulminelli and R. Raabe for fruitful discussions and advice.

[1] I. Talmi and I. Unna, Phys. Rev. Lett. **4**, 469 (1960).
[2] J. P. Deutsch *et al.*, Phys. Lett. B **28**, 178 (1968).
[3] H. Simon *et al.*, Nucl. Phys. A **734**, 323 (2004).
[4] H. Jeppesen *et al.*, Phys. Lett. B **642**, 449 (2006).
[5] H. Al Falou, A. Leprince, and N. A. Orr, J. Phys.: Conf. Ser. **312**, 092012 (2011).
[6] Y. Aksyutina *et al.*, Phys. Lett. B **666**, 430 (2008).
[7] K. K. Seth *et al.*, Phys. Rev. Lett. **58**, 1930 (1987).
[8] W. von Oertzen, Nucl. Phys. A **588**, c129 (1995).
[9] H. G. Bohlen *et al.*, Z. Phys. A Atomic Nuclei **330**, 227 (1988).
[10] H. G. Bohlen *et al.*, Prog. Part. Nucl. Phys. **42**, 17 (1999).
[11] H. Matsubara *et al.*, Few-Body Systems **54**, 1433 (2013).
[12] N. A. F. M. Poppelier *et al.*, Phys. Lett. B **157**, 120 (1985).
[13] A. A. Ogloblin, Z. Phys. A **351**, 355 (1995).
[14] H. Sagawa, Phys. Lett. B **309**, 1 (1993).
[15] H. Kitagawa, Nucl. Phys. A **551**, 16 (1993).
[16] N. A. F. M. Poppelier *et al.*, Z. Phys. A **346**, 11 (1993).
[17] L. Chen *et al.*, Phys. Lett. B **505**, 21 (2001).
[18] T. Otsuka, R. Fujimoto, Y. Utsuno, B. A. Brown, M. Honma, and T. Mizusaki, Phys. Rev. Lett. **87**, 082502 (2001).
[19] F. C. Barker, Nucl. Phys. A **741**, 42 (2004).
[20] E. K. Warburton and B. A. Brown, Phys. Rev. C **46**, 923 (1992).
[21] H. Al Falou, Ph.D. thesis, Université de Caen, 2007, http://tel.archives-ouvertes.fr/tel-00212214.
[22] H. T. Johansson *et al.*, Nucl. Phys. A **842**, 15 (2010).
[23] G. V. Rogachev *et al.*, Phys. Rev. C **67**, 041603(R) (2003).
[24] S. Fortier *et al.*, AIP Conf. Proc. **912**, 3 (2007).
[25] Y. Blumenfeld *et al.*, Nucl. Instrum. Methods Phys. Res. A **421**, 471 (1999).
[26] E. Triggestad and S. Fortier (private communication).
[27] M. S. Golovkov *et al.*, Phys. Rev. C **76**, 021605(R) (2007).
[28] E. Pollacco *et al.*, Eur. Phys. J. A **25**, 287 (2005).
[29] D. Suzuki *et al.*, Phys. Rev. Lett. **103**, 152503 (2009).
[30] X. Mougeot *et al.*, Phys. Lett. B **718**, 441 (2012).
[31] A. C. C. Villari *et al.*, Nucl. Instrum. Methods Phys. Res. B **204**, 31 (2003).
[32] T. Al Kalanee, Ph.D. thesis, Université de Caen, 2010, and references therein, http://tel.archives-ouvertes.fr/tel-00557105/.
[33] D. Suzuki, Ph.D. thesis, Department of Physics, School of Science, University of Tokyo, 2009.
[34] D. Suzuki, Eur. Phys. J. A **48**, 1 (2012).
[35] X. Mougeot, Ph.D. thesis, Université Paris VII - Denis Diderot, 2008.
[36] S. Ottini *et al.*, Nucl. Instrum. Methods Phys. Res. A **431**, 476 (1999).
[37] D. Tilley, H. Weller, and C. Cheves, Nucl. Phys. A **564**, 1 (1993).
[38] D. R. Tilley *et al.*, Nucl. Phys. A **745**, 155 (2004).
[39] M. D. Cooper *et al.*, Nucl. Phys. A **218**, 249 (1974).
[40] S. E. Darden *et al.*, Nucl. Phys. A **208**, 77 (1973).
[41] A convolution of a Lorentzian and a Gaussian distribution, see for example: R. J. Wells, J. Quant. Spectrosc. Radiat. Transfer **62**, 29 (1999).
[42] I. J. Thompson, Comput. Phys. Rep. **7**, 167 (1988).
[43] J. Lee, M. B. Tsang, and W. G. Lynch, Phys. Rev. C **75**, 064320 (2007).

[44] A. M. Lane and R. G. Thomas, Rev. Mod. Phys. **30**, 257 (1958).

[45] W. W. Daehnick, J. D. Childs, and Z. Vrcelj, Phys. Rev. C **21**, 2253 (1980).

[46] A. J. Koning and J. Delaroche, Nucl. Phys. A **713**, 231 (2003).

[47] R. V. Reid, Jr., Ann. Phys. (NY) **50**, 411 (1968).

[48] N. Keeley, N. Alamanos, and V. Lapoux, Phys. Rev. C **69**, 064604 (2004).

[49] A. F. Lisetskiy, B. R. Barrett, M. K. G. Kruse, P. Navratil, I. Stetcu, and J. P. Vary, Phys. Rev. C **78**, 044302 (2008).

[50] A. Volya and V. Zelevinsky, Phys. Rev. Lett. **94**, 052501 (2005).